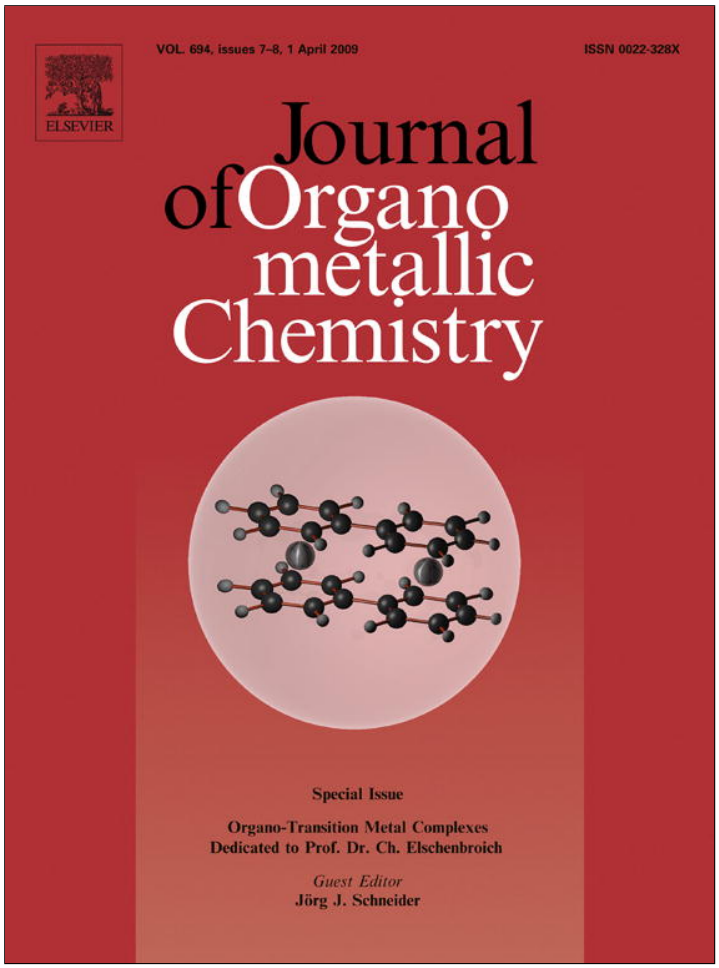

Journal of Organometallic Chemistry 694 (2009) 1069–1075

Contents lists available at ScienceDirect

Journal of Organometallic Chemistry

journal homepage: www.elsevier.com/locate/jorganchem

Synthesis of Co, Rh and Ir nanoparticles from metal carbonyls in ionic liquids and their use as biphasic liquid–liquid hydrogenation nanocatalysts for cyclohexene

Engelbert Redel [a], Jérôme Krämer [a], Ralf Thomann [b,1], Christoph Janiak [a,*]

[a] Institut für Anorganische und Analytische Chemie, Universität Freiburg, Albertstrasse 21, D-79104 Freiburg, Germany
[b] FMF (Freiburger Material Forschungszentrum), Universität Freiburg, Stefan-Meier-Strasse 21, D-79104 Freiburg, Germany

ARTICLE INFO

Article history:
Received 22 July 2008
Received in revised form 15 September 2008
Accepted 29 September 2008
Available online 2 October 2008

Dedicated to Prof. Christoph Elschenbroich on the occasion of his 70th birthday

Keywords:
Metal nanoparticles
Nanocatalysts
Catalytic olefin hydrogenation
Ionic liquids
Metal carbonyl

ABSTRACT

Stable cobalt, rhodium and iridium nanoparticles are obtained reproducibly by thermal decomposition under argon from $Co_2(CO)_8$, $Rh_6(CO)_{16}$ and $Ir_4(CO)_{12}$ dissolved in the ionic liquids $BMim^+BF_4^-$, $BMim^+OTf^-$ and $BtMA^+NTf_2^-$ [$BMim^+$ = *n*-butyl-methyl-imidazolium, $BtMA^+$ = *n*-butyl-tri-methyl-ammonium, $OTf^- = {}^-O_3SCF_3$, $NTf_2^- = {}^-N(O_2SCF_3)_2$]. The very small and uniform nanoparticle size of about 1–3 nm in $BMim^+BF_4^-$ increases with the molecular volume of the ionic liquid anion in $BMim^+OTf^-$ and $BtMA^+NTf_2^-$. Characterization of the nanoparticles was done by transmission electron microscopy (TEM), transmission electron diffraction (TED), X-ray powder diffraction (XRPD) and dynamic light scattering (DLS). The rhodium or iridium nanoparticle/IL systems function as highly effective and recyclable catalysts in the biphasic liquid–liquid hydrogenation of cyclohexene to cyclohexane with activities of up to 1900 $mol_{product}/(mol_{metal}\ h)$ and quantitative conversion within 1 h at 4 bar H_2 pressure and 75 °C.

1. Introduction

Transition-metal nanoparticles are very important for technological applications in several areas of science and industry, including catalysis or chemical sensors [1–3]. In particular, Ir and Rh nanoparticles can be used for olefin hydrogenation reactions [4]. The controlled and reproducible synthesis of defined and stable metal nanoparticles (MNPs) is of very high importance for different fields of applications [5–10]. Metal nanoparticle syntheses in ionic liquids (ILs) are carried out through the reduction [11–14] or decomposition [15] of metal salts or metal complexes, photochemical [16,17] or electro-reduction [18–20], and recently also by thermal and photochemical decomposition of metal carbonyls [21–23].

Ionic liquids stabilize metal nanoparticles on the basis of their high ionic charge, high polarity, high dielectric constant and supramolecular network [24–27]. According to DLVO (Derjaugin–Landau–Verwey–Overbeek) theory [28,29], ILs should provide an *electrosteric* protection in the form of a "*protective shell*" for MNPs, so that no extra stabilizing molecules or organic solvents are needed [30–32]. Here we note that DLVO theory treats anions as ideal point charges. Real-life anions with a molecular volume would be classified as "*electrosteric* stabilizers". However, the term "*electrosteric*" is contentious and ill-defined [33]. The stabilization of metal nanoclusters in ionic liquids could, thus, be attributed to "extra-DLVO" forces [33] including effects from the network properties of ionic liquids like hydrogen bonding, hydrophobic effects and steric interactions. However, the DLVO theory predicts that the anionic charges should be the primary source of stabilization for the electrophilic metal nanocluster. Experimentally PF_6^- anions from $BMim^+PF_6^-$ were found on a Pd nanocluster surface by XPS. This supports the hypothesis that weakly coordinating anions can contribute to the stability of transition-metal nanoclusters in organic solutions or ILs [34]. In the case of Ir nanoclusters stabilized by imidazolium ionic liquids, it was found that in addition to the BF_4 anion *N*-heterocyclic carbenes are another source of potential nanocluster stabilization in ILs [35]. Also, a correlation was found between the molecular volume of the anion in the ionic liquid and the size of the synthesized metal nanoparticles [11,21]. However, transition-metal nanoparticles in ionic liquids are only kinetically stable because the formation of bulk metal is thermodynamically favored. Yet, in the absence of strongly coordinating protective ligand layers, MNPs in ILs should be effective catalysts. The IL network contains only weakly coordinating cations and anions as stabilizers that bind less strongly to the metal surface than other anions or capping ligands. Generally, the catalytic properties

* Corresponding author. Tel.: +49 761 2036147; fax: +49 761 2036127.
E-mail addresses: ralf.thomann@fmf.uni-freiburg.de (R. Thomann), janiak@uni-freiburg.de (C. Janiak).
[1] Tel.: +49 761 2035379.

0022-328X/$ - see front matter © 2008 Elsevier B.V. All rights reserved.
doi:10.1016/j.jorganchem.2008.09.050

(activity and selectivity) of dispersed metal nanoparticles indicate that they possess pronounced surface-like (multi-site) rather than single-site-like character [1,36,37].

The hydrogenation of benzene to cyclohexane is a multi-million ton process for the subsequent oxidation of the cycloalkane to adipic acid and caprolactam as building blocks for Nylon 6.6 and Nylon 6 [38,39]. Cyclohexene is often taken as a model substrate for hydrogenation activity studies of biphasic liquid–liquid systems involving ILs [40–42], also because its solubility is limited in the polar ionic liquid $BMim^+BF_4^-$ [43]. ILs are also interesting under *green catalysis* aspects which require that catalysts be designed for easy product separation from the reaction media and multi-time catalyst recycling with very high efficiency [44]. Ionic liquids as catalytic reaction media fulfil these requirements as no surplus organic solvent is needed in biphasic catalytic transformations of liquid substrates. A low miscibility of hydrophobic substrates and products with the polar ionic liquid phase, e.g., $BMim^+BF_4^-$ allows for easy separation by simple decantation of the hydrophobic phase. Also, low-volatile products can simply be distilled off or removed under vacuum from ILs with their very low vapor pressure to allow reuse of the catalyst/IL system.

Here we report the preparation of Co, Rh and Ir-metal nanoparticles by thermal decomposition of $Co_2(CO)_8$, $Rh_6(CO)_{16}$ and $Ir_4(CO)_{12}$, respectively, in different ILs. Moreover, the synthesized nanoparticles in ILs were used as highly effective and recyclable catalysts for the biphasic liquid–liquid hydrogenation of cyclohexene to cyclohexane.

2. MNP syntheses and characterization

In a typical experiment the metal carbonyl was dissolved under argon atmosphere in the dried and deoxygenated ionic liquid (IL). The solution was heated under argon up to 230 °C (above the decomposition temperature of the metal carbonyl) for several hours in the ionic liquids *n*-butyl-tri-methylammonium *N*-bis(trifluoromethylsulfonyl)imide ($BtMA^+NTf_2^-$), *n*-butyl-methyl-imidazolium tetrafluoroborate ($BMim^+BF_4^-$) or trifluoromethanesulfonate ($BMim^+OTf^-$) (Scheme 1). $Co_2(CO)_8$ was decomposed at 180 °C, $Rh_6(CO)_{16}$ and $Ir_4(CO)_{12}$ at 230 °C. Literature reported decomposition temperatures are 220 °C for $Rh_6(CO)_{16}$, 210 °C for $Ir_4(CO)_{12}$ and above 100 °C for $Co_2(CO)_8$ [45].

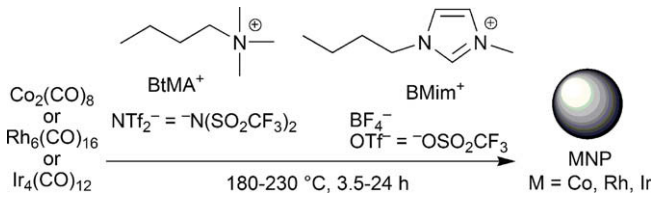

Scheme 1. Formation of Co, Rh and Ir nanoparticles by thermal decomposition of their metal carbonyls in different ionic liquids (ILs).

Dark-brown to black Co, Rh or Ir nanoparticle dispersions (Fig. S27, Supplementary material) are reproducibly obtained through decomposition from their metal carbonyl in ionic liquids (Figs. 1–4). The resulting nanoparticles were analyzed by transmission electron microscopy (TEM), transmission electron diffraction (TED), X-ray powder diffractometry (XRPD) and dynamic light scattering (DLS) (Table 1). The dispersions are found stable for more than six months under argon atmosphere. Under air the black, magnetic Co dispersion (Fig. S28) turns violet and loses its magnetic properties. The Rh and Ir dispersions are stable, and the particle size does not change, after more than 70 h with air/oxygen contact (Fig. S7 DLS). TED and XRPD studies show that the resulting Co, Rh and Ir nanoparticles produced under argon are not oxidized. The diffraction patterns correspond to their metal lattices (Fig. 5, Figs. S21–S26, Tables S2 and S3) [46], thereby proving their metal character and the absence of significant oxidation.

The median metal nanoparticle size of 3 nm for Rh and 1 nm for Ir is extremely small with a narrow or uniform, albeit not monodisperse, size distribution (Figs. 2 and 3). It is, at present, not trivial to routinely and easily prepare uniform nanoparticles of such small 1–3 nm size. No extra stabilizers or capping molecules are needed to achieve this small particle size. The size of the Co, Rh and Ir nanoparticles in $BMim^+BF_4^-$ could also be estimated with the Scherrer equation [47] from the half-width of the diffraction peaks (Figs. S24–S26). Ir nanoparticles obtained in $BMim^+OTf^-$ and $BtMA^+NTf_2^-$ range from about ~4 nm in the former to ~80 nm the later (ableit this value corresponds to large aggregates of smaller Ir nanoparticles) (Fig. 4). Co nanoparticles obtained in $BMim^+BF_4^-$ with a size of ~14 nm are magnetic and agglomerate as a result of their superparamagnetic properties (Fig. 1 and Fig. S28) [5]. The same observation of agglomerated Co nanoparticles was reported from a recent $Co_2(CO)_8$ decomposition in different imidazolium ionic liquid/hexane mixture, e.g., $BMim^+NTf_2^-$/hexane [23].

A correlation exists between the molecular volume of the anion in the ionic liquid and the synthesized metal nanoparticles [11,21,22], indicated here for, but not limited to, Rh and Ir (Fig. 6). The crystallinity and the size of the Ir nanoparticles depend on the decomposition time. The longer the dispersions were

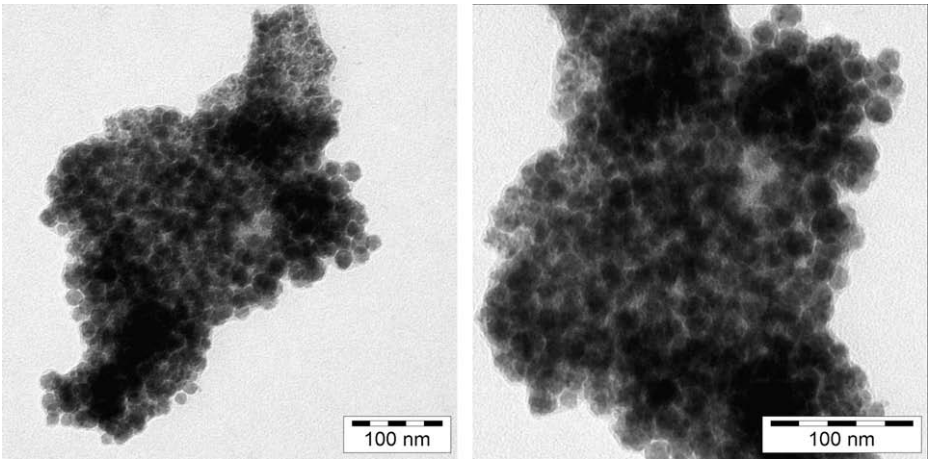

Fig. 1. Co nanoparticles from thermal decomposition of $Co_2(CO)_8$ in $BMim^+BF_4^-$ (entry 1 in Table 1).

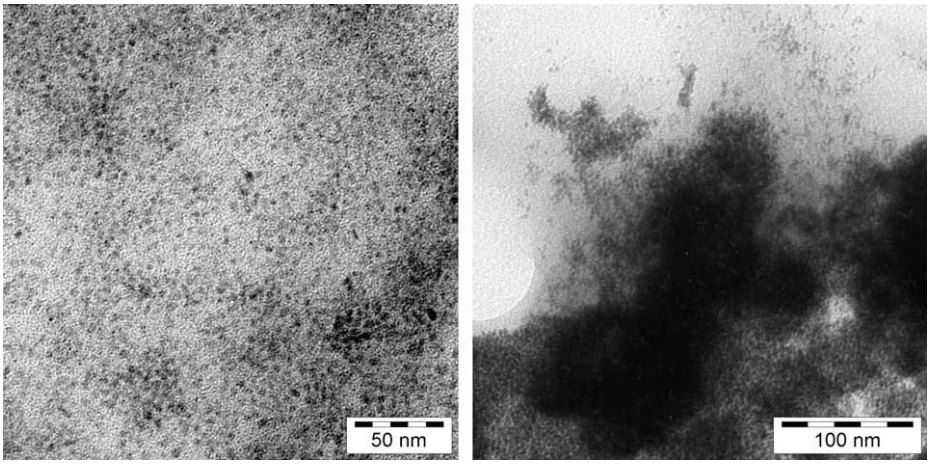

Fig. 2. Rh nanoparticles from thermal decomposition of $Rh_6(CO)_{16}$ in $BMim^+BF_4^-$ (left) and Rh nanoparticles after 6 hydrogenation cycles (right) (entry 2 and 5, respectively, in Table 1).

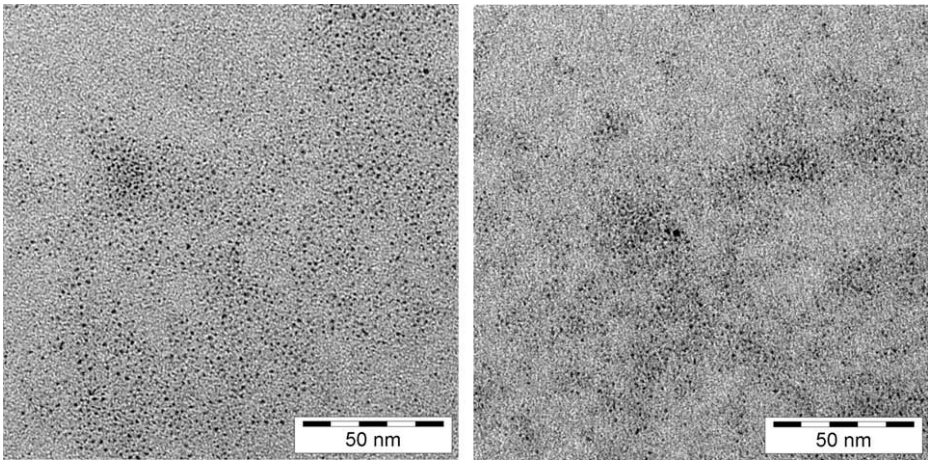

Fig. 3. Ir nanoparticles from 3.5 h (left) and 18 h (right) thermal decomposition of $Ir_4(CO)_{12}$ in $BMim^+BF_4^-$ (entry 6 and 7, respectively, in Table 1).

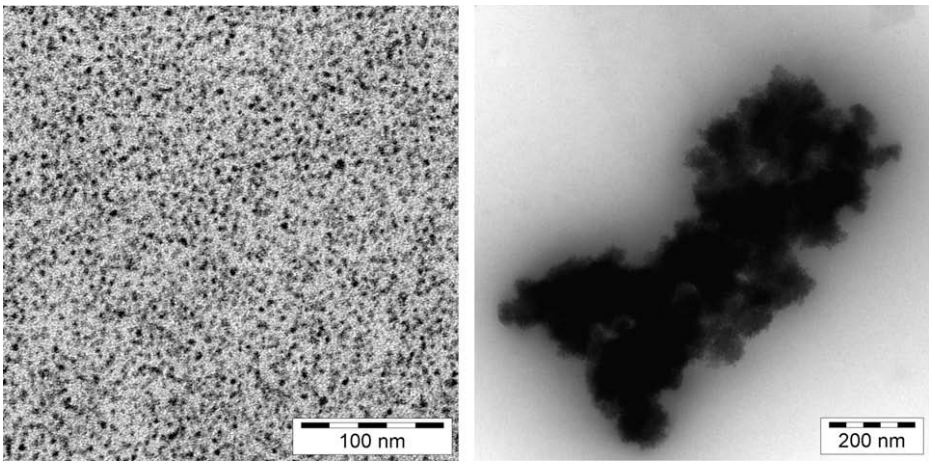

Fig. 4. Ir nanoparticles from thermal decomposition of $Ir_4(CO)_{12}$ in $BMim^+OTf^-$ (left) and $BtMA^+NTf_2^-$ (right) (entry 9 and 10, respectively, in Table 1).

heated, the more crystalline are the particles (Fig. 5). The diffraction patterns of Ir samples which have been thermolyzed for 3.5 h show only diffuse halos. Ir nanoparticles from 18 h thermolysis show narrow and well defined reflections (Fig. 5 and Fig. S23).

Nanoparticles must be stabilized in order to prevent their agglomeration or aggregation which eventually leads to the formation of small metal particles. MNPs (*core*) are considered stabilized in ILs by the formation of "*protective*" anionic and cationic layers

Table 1
MNP (M = Co, Rh and Ir) size and size distribution in different ionic liquids (ILs)

	Ionic liquid[a]	$V_{IL\text{-}Anion}$/nm^3 [56]]	Metal carbonyl/metal weight percent in IL/decomposition time	TEM median diameter/nm (standard deviation σ)[b]	Dynamic light scattering median diameter/nm (standard deviation σ)[c]
1	$BMim^+BF_4^-$	0.073 ± 0.009	$Co_2(CO)_8$/0.16/18 h	14 (±8)	
2	$BMim^+BF_4^-$	0.073 ± 0.009	$Rh_6(CO)_{16}$/0.2/18 h	3.0 (±0.6)	6.0 (±1.6)
3	$BMim^+OTf^-$	0.131 ± 0.015	$Rh_6(CO)_{16}$/0.2/18 h	4.4 (±1.1)	9.5 (±1.7)
4	$BtMA^+NTf_2^-$	0.232 ± 0.015	$Rh_6(CO)_{16}$/0.5/18 h	14 (±7)	–
5	$BMim^+BF_4^-$	0.073 ± 0.009	$Rh_6(CO)_{16}$/1/18 h[d]	3.5 (±0.8)	7.0 (±1.2)
6	$BMim^+BF_4^-$	0.073 ± 0.009	$Ir_4(CO)_{12}$/0.2/3.5 h	1.1 (±0.2)	4.1 (±0.7)
7	$BMim^+BF_4^-$	0.073 ± 0.009	$Ir_4(CO)_{12}$/0.2/18 h	1.7 (±0.3)	3.6 (±0.7)
8	$BMim^+BF_4^-$	0.073 ± 0.009	$Ir_4(CO)_{12}$/0.5/18 h	1.3 (±0.2)	3.4 (±1.0)
9	$BMim^+OTf^-$	0.131 ± 0.015	$Ir_4(CO)_{12}$/0.5/18 h	3.6 (±0.6)	7.1 (±1.1)
10	$BtMA^+NTf_2^-$	0.232 ± 0.015	$Ir_4(CO)_{12}$/0.5/18 h	81 (±23)[e]	–

[a] Solubility of metal carbonyl precursors in $BMim^+BF_4^-$ is limited to a maximum value of about 1 wt.%.
[b] Statistical evaluation of the total sample pictures (see also Supplementary material).
[c] Hydrodynamic radius, median diameter form the first 3 measurements at 633 nm. The hydrodynamic radius is roughly 2–3 times the size of the pure kernel cluster. For very small MNPs (~1 nm) the size of the hydrodynamic radius can even increase to more than 3 times the MNP radius. The resolution of the DLS instrument is 0.6 nm.
[d] After six catalytic cycles.
[e] This value corresponds to large aggregates of smaller Ir nanoparticles.

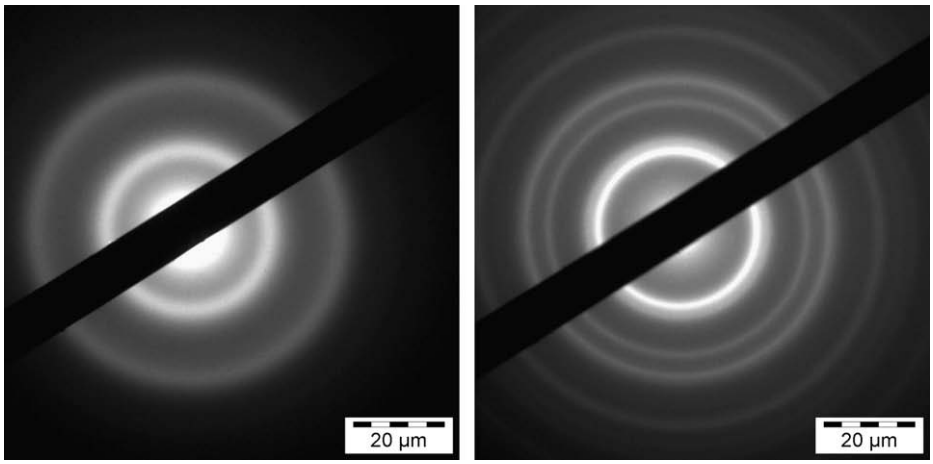

Fig. 5. Transmission electron diffraction (TED) pattern of Ir nanoparticles from $Ir_4(CO)_{12}$ in $BMim^+BF_4^-$ by thermal decomposition after 3.5 h (left) and 18 h (right) (entry 6 and 7, respectively, in Table 1). The black bar is the beam stopper. The diffraction rings at (Å) 2.2 (very strong), 1.9, 1.4, 1.2 (all strong) match with the D-spacing of the Ir-metal diffraction pattern (see Fig. S23 and Table S3).

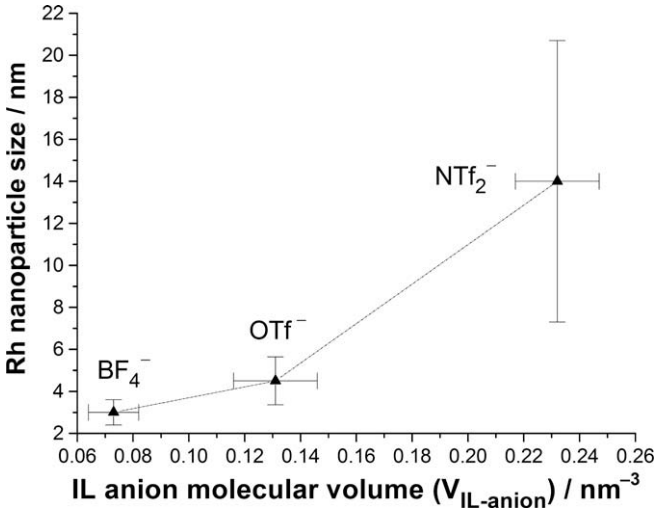

Fig. 6. Correlation between the molecular volume of the ionic liquid anion ($V_{IL\text{-}anion}$) and the observed Rh nanoparticle size with standard deviations as error bars (from TEM measurements, entry 2–4 in Table 1).

(*shells*) around them in a "*core-shell system*" [30,48–51]. According to DLVO theory the first inner shell must be anionic [28]: Then the IL anion will have the highest influence on the size and electrostatic stabilization of the Co, Rh and Ir nanoparticle. The anion molecular volume determines the region of the nanoparticle size (Fig. 6), although the supramolecular imidazolium-anion clusters of ILs should be taken into account [11,21]. Pure ILs can be regarded as supramolecular polymeric structures with a high degree of self-organisation and weak interactions of an extended network of cations and anions connected together by hydrogen bonds [6]. When mixed with other molecules or MNPs, ionic liquids become nano-structured materials with polar and nonpolar regions [6,52–55]. The ionic liquid represents an excellent medium for the formation of MNPs with, in most cases, a small size and size distribution under mild conditions.

3. Cyclohexene hydrogenation catalysis with MNP/IL

The obtained Co, Rh and Ir nanoparticle/IL dispersions were tested for their catalytic activity in the biphasic liquid–liquid hydrogenation of cyclohexene to cyclohexane (Scheme 2 and Table 2).

Scheme 2. Hydrogenation of cyclohexene catalyzed by Co, Rh and Ir nanoparticles in $BMim^+BF_4^-$.

Table 2
Catalytic biphasic liquid–liquid hydrogenation of cyclohexene to cyclohexane with MNP (M = Co, Rh or Ir) in $BMim^+BF_4^-$ ionic liquid

	Dispersion (metal wt.%)	Molar ratio cyclohexene/metal	Reaction temperature (°C)	Time (h)	Conversion (%)	Activity mol product (mol metal)$^{-1}$ h^{-1}
1[a]	Co 0.8	60	80	3	0.8	0.16
2[a]	Co 0.8	60	90	18	1.1	0.04
3[b]	Rh 0.2	1000	75	2.5	95	380
4[c]	Rh 1	80	75	2.5	98	32
5[b]	Rh 0.2	1000	75	2.5	75	300
6[b]	Rh 0.2	1000	75	2.5	93	370
7[b]	Ir 0.2	2000	75	1	97	1940
8[b]	Ir 0.2	2000	75	2.5	100	800
9[b]	Ir 0.2	2000	75	1	90	1800
10[b]	Ir 0.2	2000	75	1	80	1600

[a] 0.5 ml CoNP/IL dispersion (c = 0.166 mol/l) and 0.5 ml cyclohexene.
[b] 0.08 ml MNP/IL dispersion (M = Rh, c = 0.025 mol/l; M = Ir, c = 0.0128 mol/l) and 0.2 ml cyclohexene.
[c] 1.0 ml RhNP/IL dispersion and 1.0 ml cyclohexene. Cyclohexene density = 0.811 g/ml, M = 82.14 g/mol, 1.0 ml corresponds to 10 mmol. $BMim^+BF_4^-$ density = 1.21 g/ml.

While the Co nanoparticles showed very little to no activity (Table 2), Ir and Rh nanoparticles were found to be highly active nanocatalysts under very mild reaction conditions (75 °C, 4 bar H_2 pressure). Especially Ir nanoparticles exhibited very high catalytic activities of up to 1900 mol product (mol metal)$^{-1}$ h^{-1}. Rh nanoparticles showed good catalytic activities in the range of 300–380 mol product (mol metal)$^{-1}$ h^{-1} through different catalytic runs (Table 2). The higher catalytic activity of Ir in comparison to Rh nanoparticles may be explained by their somewhat smaller size and concomitant lager surface-to-volume ratio (cf. Table 1). During our studies it became evident that the glass vessels need to be carefully cleaned with conc. HCl/HNO_3 mixture (aqua regia) followed by surface passification with Me_3SiCl to avoid both catalyst transfer by glass surface adsorption and partial catalyst deactivation, respectively. Cyclohexene conversions of over 50% could still be observed without any new catalyst addition or with normally low active CoNP/IL when the glass vessel was only washed with acetone, water and isopropanol but no acid treatment following a Rh- or IrNP/IL run. On the other hand, the high activity of IrNP/IL was significantly lowered without the Me_3SiCl glass surface passification after the acid treatment.

Activity calculations with metal nanoparticles are typically based on the total amount of metal and not only the surface metal part. Different studies show that the catalytic activity results not only from the exposed surface metal atoms. During heterogeneous catalysis the surface can restructure and atoms can shift positions. These changes in the surface lead to a difficult to determine number of surface atoms. Partial aggregation is also possible during catalysis which would have a strong influence on the fraction of the surface atoms. Heterogeneous catalytic reactions are extremely complex and it is also possible that atoms under the exposed surface atoms play a significant role in the catalytic activity. Moreover, defects, the surface topology and surface atom sites (edges, corners, steps) rather than the sole amount of surface atoms strongly influence the catalytic activity [57].

In the context of *green catalysis* aspects the recyclability of the MNP/IL system was investigated. The biphasic liquid–liquid catalytic hydrogenation of cyclohexene could utilize the low miscibility of the hydrophobic substrate and product (cyclohexene and cyclohexane [43]) with the polar ionic liquid phase $BMim^+BF_4^-$ for phase separation by decantation. With our small volumes this procedure proved not very practical, however, and complete organic phase separation could not be ensured this way. Hence, we separated the cyclohexene/cyclohexane mixture by distillation from the low-volatile IL phase. Based on the conditions for entry 4 in Table 2 the catalysis was started with 0.08 ml RhNP/$BMim^+BF_4^-$ dispersion (c = 0.025 mol/l; and 0.2 ml (2 mmol) cyclohexene (molar cyclohexene/metal ratio = 1000)) at 75 °C and 4 bar H_2 pressure. After 2.5 h the organic phase was distilled off and fresh cyclohexene substrate (0.2 ml) was added. It is evident that the RhNP/$BMim^+BF_4^-$ dispersion can be reused more than six times without any significant loss in catalytic activity (see Scheme 3), contrary to reports in the literature where RhNP was prepared from $RhCl_3 \cdot 3H_2O$ through H_2 reduction in $BMim^+PF_6^-$ [13]. In the absence of a scavenger the reduction route will generate HCl. Also, the PF_6^- anion is known to more easily decompose to HF than BF_4^- in the presence of water and/or metal [58–61]. The formation of acids in ILs is disadavantages for the NP/IL network stability because of proton incorporation in the IL dynamic matrix [11]. With our RhNP/$BMim^+BF_4^-$ dispersion there may even be a *small* activity increase through the first cycles (see Scheme 3). This should not be over interpreted for the moment as the activity increase from 350 (1st cycle, 88% conversion) to 400 mol product (mol metal)$^{-1}$ h^{-1} (6th cycle, quantitative conversion) can be seen to fluctuate around 375 mol product (mol metal)$^{-1}$ h^{-1} with some measurement errors (from GC). Still, some activity increase could be reasoned by the formation of Rh-hydride species and their immediate presence in subsequent cycles which prevents an induction time and, thereby speeds up the reaction. Furthermore, a TEM and DLS investigation of the Rh nanoparticles after six catalytic cycles, albeit based on a 1 wt.% RhNP dispersion (entry 5 in Table 1 and Fig. 2, right, see also Figs. S4, S14 and S15) indicates particle agglomeration regions of smaller particles, yet the individual small particles can still be seen. With the 0.2 wt.% RhNP/IL solution used in catalysis the agglomeration is likely to be less and the expected concomitant activity loss apparently outweighted by the formation of more active (Rh-hydride) surface species.

The catalytic activity of RhNPs prepared from $Rh_6(CO)_{16}$ in $BMim^+BF_4^-$ can be compared with other cyclohexene hydrogenation catalysts and their precursors in Table 3. It is evident from

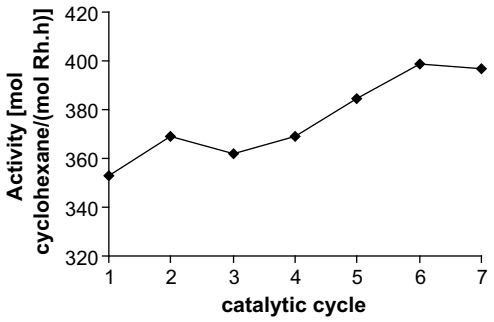

Scheme 3. Activity over seven catalytic cycles for the hydrogenation of cyclohexene (0.2 ml, 2 mmol) with the same 0.2 metal wt.% RhNP/$BMim^+BF_4^-$ catalyst (0.08 ml, 0.002 mmol) and molar cyclohexene/metal ratios of 1000 at 75 °C, 4 bar H_2 pressure and 2.5 h reaction time. An activity of 350 mol product (mol metal)$^{-1}$ h^{-1} corresponds to 88% and an activity of 400 to quantitative (100%) conversion.

Table 3
Catalyst activities of MNPs in the biphasic liquid–liquid cyclohexene hydrogenation with $BMim^+$ containing ILs

Precursor/MNP	Ionic liquid anion	Activity mol product $(mol\ metal)^{-1}\ h^{-1}$	Reference
$[IrCl(cod)]_2$/Ir	PF_6^-	343	[40]
[Ru(cod)(cot)]/Ru	BF_4^-	100	[43]
	PF_6^-	62	
RuO_2/Ru	BF_4^-	388	[41]
	PF_6^-	943	
	PF_6^-	147	
$Pd(acac)_2$/Pd	PF_6^-	143	[42]

the data in Table 3 that the catalytic properties of MNP/ILs are influenced by the nature of the IL anion [31]. The catalytic activity of IrNPs from $Ir_4(CO)_{12}$ is remarkably higher than that of Ir nanoparticles made by hydrogen reduction of $[IrCl(cod)]_2$ [40]. We suggest that the reduction route leads to, e.g., HCl impurities in the ionic liquid which lower its stabilization effect and result in catalyst deactivation. The carbonyl decomposition route helps to avoid any alteration of the IL phase. We note that in solvents other than ILs, acids can have a positive effect on the catalyst activity. This was shown, for example, in the acetone hydrogenation carried out in neat acetone with IrNP (generated from IrCl(1,5-cod)/H_2, thereby yielding one equivalent of HCl) [62].

4. Conclusions

We describe here a simple and reproducible metal carbonyl thermolysis for the synthesis of stable Co, Rh and Ir-metal nanoparticles in ionic liquids, in particular in $BMim^+BF_4^-$, with rather small and uniform MNP sizes of about 1–3 nm for Rh and Ir nanoparticles. No extra stabilizers or capping molecules are needed to achieve this small particle size. The synthesis uses easily commercially available metal carbonyl precursors and can readily be expanded to the broad range of other metal carbonyl complexes. ILs are once again demonstrated to present a favorable template for the preparation of predictable chemical nanostructures. Furthermore, the obtained RhNP and IrNP/IL dispersions were employed as highly active and reusable "*green catalysts*" without the need of other organic solvents in the biphasic liquid–liquid hydrogenation of cyclohexene.

5. Experimental

Materials and Instrumentation: $Co_2(CO)_8$, $Rh_6(CO)_{16}$, and $Ir_4(CO)_{12}$ were obtained from Strem, ionic liquids *n*-butyl-tri-methylammonium bis(trifluoromethylsulfonyl)imide ($BtMA^+NTf_2^-$), *n*-butyl-methyl-imidazolium tetrafluoroborate ($BMim^+BF_4^-$) and trifluoromethanesulfonate ($BMim^+OTf^-$) from IoLiTec (H_2O content $\ll$ 100 ppm; Cl^- content $\ll$ 50 ppm). Chloride anion impurities could be another possible source of the stabilization of metal nanoclusters in ionic liquids [33]. Because of the certified small chloride content in our commercial ILs, the Cl anions will only have a minor role, if any, for such MNP stabilization. All manipulations were done using Schlenk techniques under argon since the metal carbonyls are hygroscopic and air sensitive. The ionic liquids were dried at high vacuum (10^{-3} mbar) for several days to avoid especially in the case of $BMim^+BF_4^-$ the hydrolysis to HF [58–61].

Transmission electron microscopy (TEM) photographs were taken at room temperature from a carbon-coated copper grid on a Zeiss LEO 912 transmission electron microscope operating at an accelerating voltage of 120 kV.

Powder X-ray diffractograms were measured at ambient temperature using a STOE STADI-P with Debye–Scherrer geometry, Mo Kα radiation (λ = 0.7093 Å), a Ge(1 1 1) monochromator and the samples in glass capillaries on a rotating probe head. Simulated powder patterns were based on single-crystal data and calculated using the STOE WINXPOW software package [46].

A Malvern Zetasizer Nano-ZS was used for the dynamic light scattering measurements working at 633 nm wavelength. Care was taken for choosing the right parameters, such as the index of refraction of Co (2.8), Rh (1.7) and Ir (2.3) each at 0.1 absorption at their wavelength. Samples were prepared by dilution of 50 μL (0.2 wt.% of M); 10 μL (1 wt.% of M) of the metal/IL dispersion in 2 mL *n*-butyl-imidazole (99% p.a.; particle free). Hundred and fifty microliters of this M/IL/*n*-butyl-imidazole solution were diluted further with 1.5 mL *n*-butyl-imidazole in a glass cuvette before measurement.

5.1. Metal nanoparticle syntheses

Thermal decompositions were carried out under argon in a glass vessel which was connected to an oil bubbler. In a typical experiment (see Tables 1 and 4) the metal carbonyl was dissolved/dispersed (during ~1 h) under argon at room temperature in 3.0 g of the ionic liquid to give a solution/suspension with a defined weight percentage (wt.%) in metal. The solution was slowly heated to 180 °C (Co) or 230 °C (Rh, Ir) for 18 h under stirring. After cooling to room temperature under argon an aliquot of the ionic liquid was collected under argon atmosphere for *in situ* TEM, TED and dynamic light scattering characterization.

5.2. Catalysis

Catalytic reactions were carried out either in a 120 ml Büchi glass autoclave or in a 30 ml glass inlay within a steel autoclave at 4 bar H_2 pressure (constant pressure setting for Rh and Ir, initial pressure for Co) and 75 °C. Cylohexene was added to the metal-dispersions under argon. The ionic liquid containing the particles and the substrate formed a biphasic system. The ionic liquid is the lower, more dense phase with the Co, Rh or Ir nanoparticles, the upper phase is the cyclohexene/cyclohexane. During the reaction at 75 °C a homogenous, single liquid phase was obtained. After cooling to room temperature phase separation occured again. The cyclohexene to cyclohexane conversion was analyzed by putting a drop of the mixture into a GC sample vial with 1 ml of water. The addition of water as a non-electrolyte can enlarge the activity coefficient of organic components, thereby increase their detection sensitivity through the increase in peak area. The FID does not detect the water itself [63]. The vial was closed with aluminum crimp caps (with butyl rubber septum), placed into the headspace sampler (thermostated for 20 min to 50 °C) of a GC-headspace Perkin–Elmer 8500 HSB 6, equipped with a DB-5 film capillary column

Table 4
Decomposition conditions and experimental data for MNP synthesis

	Metal carbonyl	Ionic liquid[a]	Metal (wt.%)	Mass metal carbonyl (mg)	Decomposition temperature (°C)
1a	$Co_2(CO)_8$	$BMim^+BF_4^-$	0.16	14	180
1b	$Co_2(CO)_8$	$BMim^+BF_4^-$	0.8	71	180
2	$Rh_6(CO)_{16}$	$BMim^+BF_4^-$	0.2	11	230
3	$Rh_6(CO)_{16}$	$BMim^+OTf^-$	0.2	11	230
4	$Rh_6(CO)_{16}$	$BtMA^+NTf_2^-$	0.5	26	230
5	$Rh_6(CO)_{16}$	$BMim^+BF_4^-$	1	52	230
6	$Ir_4(CO)_{12}$	$BMim^+BF_4^-$	0.2	9	230
7	$Ir_4(CO)_{12}$	$BMim^+BF_4^-$	1	43	230
8	$Ir_4(CO)_{12}$	$BMim^+BF_4^-$	0.5	21	230
9	$Ir_4(CO)_{12}$	$BMim^+OTf^-$	0.5	21	230
10	$Ir_4(CO)_{12}$	$BtMA^+NTf_2^-$	0.5	21	230

[a] 3.0 g ionic liquid.

(60 m × 0.32 mm, film thickness 25 μm, oven temperature 60 °C, N_2 carrier flow 114 l/min) and a flame ionization detector (FID, 250 °C detector temperature). After the thermostatization time a sample was automatically drawn from the gas phase in the vial. The product was analyzed by the GC retention time versus authentic samples of cyclohexene and cyclohexane. Hydrogenation conversion (%) was calculated from the obtained cyclohexane-to-cyclohexene peak area and compared to a calibration curve from different ratios of given cyclohexene/cyclohexane mixtures which had been measured under identical headspace conditions.

Acknowledgment

We thank Dr. T.J.S. Schubert from IoLiTec (Ionic Liquids Technologies GmbH, Denzlingen, Germany) for donation of ionic liquids.

Appendix A. Supplementary material

Supplementary material available: Statistical graphs for dynamic light scattering, additional TEM and TED pictures, X-ray powder diffractograms, photographs of MNP/IL dispersions. Supplementary data associated with this article can be found, in the online version, at doi:10.1016/j.jorganchem.2008.09.050.

References

[1] V.I. Pârvulescu, C. Hardacre, Chem. Rev. 107 (2007) 2665.
[2] R. Elghanian, J.J. Storhoff, R.C. Mucic, R.L. Letsinger, C.A. Mirkin, Science 277 (1997) 1078.
[3] J.A. Alonso, Chem. Rev. 100 (2000) 637;
H. Haberland, Clusters of Atoms and Molecules, Springer, Berlin, 1994.
[4] P. Braunstein, J. Rosé, in: P. Braunstein, L.A. Oro, P.R. Raithby (Eds.), Metal Clusters in Chemistry, vol. 2, Wiley-VCH, Weinheim, 2001, pp. 616–677 (Chapter 2).
[5] A.H. Lu, E.L. Salabas, F. Schüth, Angew. Chem., Int. Ed. 46 (2007) 1222.
[6] A. Gedanken, Ultrason. Sonochem. 11 (2004) 47.
[7] C.N.R. Rao, S.R.C. Vivekchand, K. Biwas, A. Govindaraj, Dalton Trans. (2007) 3728.
[8] Y. Mastai, A. Gedanken, in: C.N.R. Rao, A. Müller, A.K. Cheetham (Eds.), Chemistry of Nanomaterials, vol. 1, Wiley-VCH, Weinheim, 2004, p. 113ff.
[9] D. Mahajan, E.T. Papish, K. Pandya, Ultrason. Sonochem. 11 (2004) 385.
[10] J. Park, J. Joo, S.G. Kwon, Y. Jang, T. Hyeon, Angew. Chem., Int. Ed. 46 (2007) 4630.
[11] E. Redel, R. Thomann, C. Janiak, Inorg. Chem. 48 (2008) 14.
[12] T. Gutel, J. Garcia-Antón, K. Pelzer, K. Philippot, C.C. Santini, L.S. Ott, R.G. Finke, Inorg. Chem. 45 (2006) 8382.
[13] G.S. Fonseca, A.P. Umpierre, P.F.P. Fichtner, S.R. Teixeira, J. Dupont, Chem. Eur. J. 9 (2003) 3263.
[14] Z. Li, A. Friedrich, A. Taubert, J. Mater. Chem. 18 (2008) 1008.
[15] P. Migowski, G. Machado, L.M. Rossi, G. Machado, J. Morais, S.R. Teixeira, M.C.M. Alves, A. Traverse, J. Dupont, Phys. Chem. Chem. Phys. 9 (2007) 4814.
[16] J.M. Zhu, Y.H. Shen, A.J. Xie, L.G. Qiu, Q. Zhang, X.Y. Zhang, J. Phys. Chem. C 111 (2007) 7629.
[17] M.A. Firestone, M.L. Dietz, S. Seifert, S. Trasobares, D.J. Miller, N.J. Zaluzec, Small 1 (2005) 754.
[18] K. Peppler, M. Polleth, S. Meiss, M. Rohnke, J.Z. Janek, Phys. Chem. 220 (2006) 1507.
[19] A. Safavi, N. Maleki, F. Tajabadi, E. Farjami, Electrochem. Commun. 9 (2007) 1963.
[20] K. Kim, C. Lang, P.A. Kohl, J. Electrochem. Soc. 152 (2005) E9.
[21] E. Redel, R. Thomann, C. Janiak, Chem. Commun. (2008) 1789.
[22] J. Krämer, E. Redel, R. Thomann, C. Janiak, Organometallics 27 (2008) 1976.
[23] D.O. Silva, J.D. Scholten, M.A. Gelesky, S.R. Teixeira, A.C.B. Dos Santos, E.F. Souza-Aguiar, J. Dupont, ChemSusChem 1 (2008) 291.
[24] A. Taubert, Z. Li, Dalton Trans. (2007) 723.
[25] J. Dupont, J. Brazil. Chem. Soc. 15 (2004) 341.
[26] C.S. Consorti, P.A.Z. Suarez, R.F. de Souza, R.A. Burrow, D.H. Farrar, A.J. Lough, W. Loh, L.H.M. da Silva, J. Dupont, J. Phys. Chem. B 109 (2005) 4341.
[27] J. Dupont, P.A.Z. Suarez, R.F. de Souza, R.A. Burrow, J.P. Kintzinger, Chem. Eur. J. 6 (2000) 2377.
[28] E.J.W. Verwey, J.T.G. Overbeek, Theory of the Stability of Lyophobic Colloids, 2nd ed., Dover Publications Mineola, New York, 1999.
[29] B.W. Ninham, Adv. Colloid Int. Sci. 83 (1999) 1.
[30] G. Schmidt, Nanoparticles, Wiley-VCH, Weinheim, 2004.
[31] D. Astruc, F. Lu, J.R. Aranzaes, Angew. Chem., Int. Ed. 44 (2005) 7852.
[32] M. Antonietti, D. Kuang, B. Smarly, Y. Zhou, Angew. Chem., Int. Ed. 43 (2004) 4988.
[33] L.S. Ott, R.G. Finke, Coord. Chem. Rev. 251 (2007) 1075.
[34] A.P. Umpierre, G. Machado, G.H. Fechner, J. Morais, J. Dupont, Adv. Synth. Catal. 347 (2005) 1404.
[35] J.D. Scholten, G. Ebeling, J. Dupont, Dalton Trans. (2007) 5554.
[36] D. Astruc, Nanoparticles and Catalysis, Wiley, New York, 2007.
[37] A. Roucoux, J. Schulz, H. Patin, Adv. Synth. Catal. 345 (2003) 222.
[38] H.-G. Elias, Makromoleküle, Band 3, Industrielle Polymere und Synthesen, Wiley-VCH, Weinheim, 2001.
[39] B.K. Hodnett, Heterogenous Catalytic Oxidations, Wiley, New York, 2000.
[40] J. Dupont, G.S. Fonseca, A.P. Umpierre, P.F.P. Fichtner, S.R. Texeira, J. Am. Chem. Soc. 124 (2002) 4228.
[41] L.M. Rossi, G. Machado, P.F.P. Fichtner, S.R. Teixeira, J. Dupont, Catal. Lett. 92 (2004) 149.
[42] J. Huang, T. Jiang, B. Han, H. Gao, Y. Chang, G. Zhao, W. Wu, Chem. Commun. (2003) 1654.
[43] E.T. Silveira, A.P. Umpierre, L.M. Rossi, G. Machado, J. Morais, G.V. Soares, I.L.R. Baumvol, S.R. Teixeira, P.F.P. Fichtner, J. Dupont, Chem. Eur. J. 10 (2004) 3734.
[44] D.J. Adams, P.J. Dyson, S.J. Travener, Chemistry in Alternative Reaction Media, Wiley, New York, 2004.
[45] A.F. Holleman, N. Wiberg, Lehrbuch der Anorganischen Chemie, 102nd ed., Walter de Gruyter, Germany, Berlin, 2007.
[46] STOE WINXPOW version 1.10, data base, STOE & Cie GmbH, Darmstadt, Germany, 2002.
[47] R. Allmann, Röntgenpulverdiffraktometrie, Springer, Berlin, 2005.
[48] A.N. Shipway, E. Katz, I. Willner, ChemPhysChem 1 (2000) 18.
[49] T. Cassagneau, J.H. Fendler, J. Phys. Chem. B 103 (1999) 1789.
[50] C.D. Keating, K.K. Kovaleski, M.J. Natan, J. Phys. Chem. B 102 (1998) 9404.
[51] E. Redel, J. Krämer, R. Thomann, C. Janiak, GIT Labor-Fachzeitschrift (04) (2008) 400.
[52] T.J. Gannon, G. Law, R.P. Watson, A.J. Carmichael, K.R. Seddon, Langmuir 15 (1999) 8429.
[53] G. Law, R.P. Watson, A.J. Carmichael, K.R. Seddon, Phys. Chem. Chem. Phys. 3 (2001) 2879.
[54] J.N.C. Lopes, M.F.C. Gomes, A.A.H. Padua, J. Phys. Chem. B 110 (2006) 16816.
[55] J.N.C. Lopes, A.A.H. Padua, J. Phys. Chem. B 110 (2006) 3330.
[56] I. Krossing, J.M. Slattery, Z. Phys. Chem. 220 (2006) 134.
[57] G. Ertl, H. Knözinger, J. Weitkamp, Handbook of Heterogonous Catalysis vols. 1–8, 2nd ed., Wiley-VCH, Weinheim, Germany, 2008.
[58] F. Endres, S.Z. El Abedin, Phys. Chem. Chem. Phys. 8 (2006) 2101.
[59] P. Wasserscheid, T. Welton, Ionic Liquids in Synthesis vol. 1, 2nd ed., Wiley-VCH, Weinheim, 2007.
[60] R.P. Swatloski, J.D. Holbrey, R.D. Rogers, Green Chem. 5 (2003) 361.
[61] G.A. Baker, S.N. Baker, Aust. J. Chem. 58 (2005) 174.
[62] S. Özkar, R.G. Finke, J. Am. Chem. Soc. 127 (2005) 4800.
[63] H. Hachenberg, K. Beringer, Die Headspace-Gaschromatographie als Analysen- und Meßmethode, Vieweg, Braunschweig/Wiesbaden, Germany, 1996, pp. 32–35.